MAGNETIC AND ELECTROCONDUCTIVE PROPERTIES OF THE PURE CARBON SOOT SYNTHESISED BY ARC DISCHARGE

Zaikovskii A.V. PhD.[1]
Kutateladze Institute of Thermophysics SB RAS, Ac. Lavrentiev Ave. 1, 630090, Novosibirsk, Russia [1]

lexeyza@gmail.com

Abstract: *The electroconductive and magnetic properties of nanomaterials containing carbon nanoforms synthesised for electrocatalytic, electrochromic, and ferrofluid applications, etc., are of interest to researchers. This article aims to understand the physical effects influencing the electroconductive and magnetic properties of materials synthesised by arc discharge. The nanomaterial formation processes leading to the formation of magnetic and electroconductive structures are also discussed. Arc discharge between graphitic electrodes results in the emergence of a fan-shaped jet of helium and carbon. The gasdynamic and temperature parameters of the jet depend on the parameters of the arc discharge and the buffer gas. Variations in the parameters of the carbon vapour flow change the kinetics of carbon condensation, leading to variations in the morphology and structure of the carbon material. The main external parameter of the synthesis (buffer gas pressure) was varied in the study, and correlations between the intensity ratio of the D to G peaks on the Raman spectrum and the electrical conductivity and magnetic susceptibility values were found. During the synthesis, nanographite structures were formed. However, the formation of an amorphous carbon structure on the free 'zig-zag' edges of the graphite fragments reduced the magnetic susceptibility, the electrical conductivity and the ID/IG ratio.*

Keywords: ARC-DISCHARGE, CARBON NANOMATERIALS, ELECTRICAL CONDUCTIVITY, MAGNETIC SUSCEPTIBILITY

1. Introduction

The current interest in nanostructured materials is due to their unique properties and potential applications. One of the bottom-up physical methods for nanomaterial synthesis is arc discharge which results in sputtering of the electrode materials and a condensation process that leads to nanoparticle formation.

Arc discharge between coaxial graphite electrodes results in the formation of a fan-shaped jet emerging from the interelectrode gap. This jet consists of buffer gas and the products of graphite sputtering [1, 2]. Variation in the external discharge conditions leads to changing parameters in the discharge plasma and the fan-shaped jet.

The arc discharge method allows synthesis metallic [3, 4] and composite [5, 6] nanoparticles stabilised by a carbon matrix. This method prevents the coagulation of the nanoparticles and, correspondingly, the increase in size and loss of reactivity of the nanoparticles. Many parameters of the synthesised materials depend on the properties of the carbon matrix.

Electroconductivity influences the electrocatalytic [6] and electrochromic [7] applications of synthesised nanomaterials. Electrical conductivity, in turn, depends on the consistency and structure of the carbon. For wide-gap semiconductors in the case of diamond structures consisting of sp^3-hybridised carbon atoms, this value is ~10^{-13} S/m. On the other hand, the metallic conductivity value for the parallel orientation of graphitic layers consisting of sp^2-hybridised carbon atoms is ~10^5 S/m.

The magnetic properties of the carbon matrix are of interest for applications relating to ferrofluid creation [8], bio-inert magnetic materials and others. Magnetic properties and electroconductive properties depend on the internal structure of the carbon material [9]. Both the core of the carbon atom [10] and bulk forms such as graphite [11, 12] and diamond [13] have diamagnetic properties. The same is true for nanoscale carbon forms such as nanotubes [14] and fullerenes [15]. Paramagnetism and even ferromagnetism at room temperature have been predicted and discovered in such forms as nanotubes in a closed torus [16] and nanofragments of graphite [17]. In the case of nanographite, paramagnetism is determined by the presence of free 'zig-zag' edges that lead to the formation of unusually high Fermi level density states [18, 19], which in turn leads to increases in Pauli paramagnetism [20].

Various parameters of arc discharge synthesis determine the structural features of the carbon material such as fullerenes [21], graphene [22, 23], carbon nanotubes [24], etc. The most common product of arc discharge sputtering of the graphite electrodes is carbon soot, which consists of sp^2-, sp^3-hybridised carbon atoms [25]. The main effects on the structure of the material are caused by the buffer gas pressure in the reactor chamber. The present study examines the effects of buffer gas pressure on the electroconductive and magnetic properties of synthesised carbon materials.

The aim of this study is to investigate the electroconductive and magnetic properties of carbon materials synthesised at the discharge parameters used for nanoparticle synthesis.

2. Materials and methods

The carbon materials were synthesised using a plasma-chemical reactor presented on Fig. 1. The reactor consists of a sealed chamber (1). A movable graphite cathode (2) is mounted in the chamber. Solid graphite rod used as sprayed anode (3) is mounted coaxial with the cathode. The amount of impurities of used graphite was less than 1 ppm, and the amount of Fe less than 0.1 ppm. Helium was used as the buffer gas. The reactor chamber was first purged by helium then filled with helium at a certain pressure. The experiments were carried out with a consistent direct current of 120 A supplied by DC source (4), and the buffer gas pressure ranged from 3 to 200 Torr. Arc discharge is ignited between the electrodes, which results in spraying of the anode. The arc discharge voltage is stabilised with help of a voltmeter (5) and screw assembly (6). Spraying of the anode results on the evaporation of graphite and emergence of the carbon atoms and clusters in the discharge area. Flows of the sputtered graphite products and helium from electrode gap to the reactor chamber result in carbon condensation and nanoparticle formation. Synthesised carbon material is collected on water cooled screen (7). The experiments were carried out on various buffer gas pressure ranged from 3 to 200 Torr. The buffer gas pressures are controlled with help of digital pressure sensor (8) and solenoid valve (9) controlled by a control board (10).

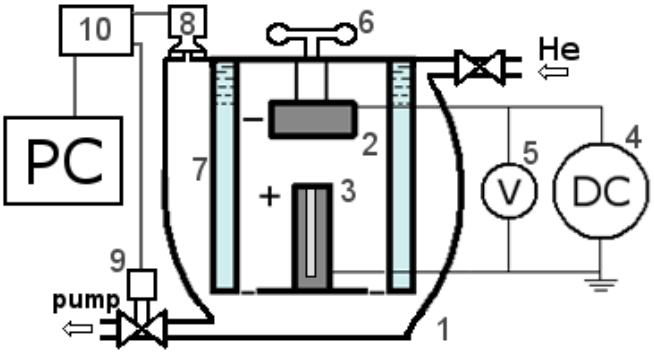

Fig.1. *Set-up of plasma-chemical reactor*

WEB ISSN 2535-0226
PRINT ISSN 2535-0218

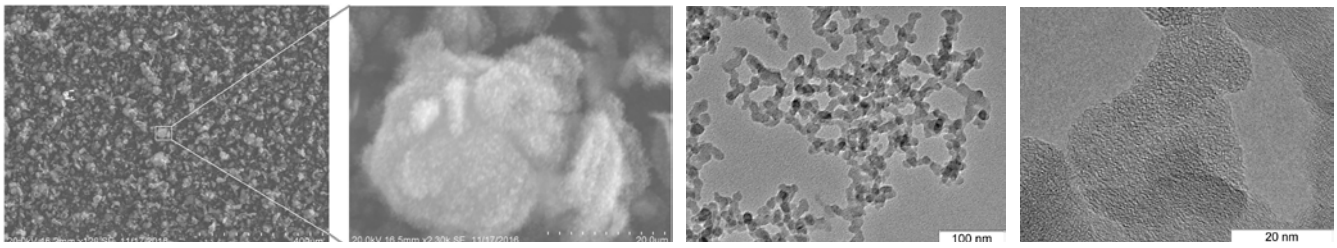

Fig. 2. *(a) SEM image of the deposited carbon layer, (b) SEM image of the single agglomerate, (c) TEM image of the chains carbon globules, (d) HRTEM image of the single carbon globule.*

Synthesised carbon nanomaterials were labelled *C3, C6, C12, C25, C50, C100* and *C200*, with these numbers corresponding to the pressure in Torr.

The magnetic properties of the synthesised nanomaterials were studied at room temperature using a SM-150L magnetic susceptibility meter (ZH instruments, Czech Republic) with a working frequency of 16 kHz and a stretch field of 320 A/m.

The electrical conductivity of the synthesised materials was studied using resistivity analysis while compressing the materials between parallel flat copper contacts. The density was determined by dividing the mass of the tested material by the filled volume.

Scanning electron microscopy (SEM) was carried out using a S-3400N microscope (Hitachi Science Systems Ltd., Japan) in secondary electron detection mode. The size distributions were plotted according to the sizes of the carbon agglomerates measured from the SEM images.

Transmission electron microscopy (TEM) was carried out using a JEM-2010 microscope (JEOL Ltd., Japan). The size distributions were plotted according to the sizes of the nanoparticles measured from the TEM images.

Raman spectroscopy was carried out using a Spex Triplemate Raman spectrometer (Princeton Instruments, USA) equipped with an LN-1340 PB multi-channel detector.

3. Results and discussion

After synthesis the materials that were produced were deposited on the product-gathering screen forming a low-density carbon layer. The layer consisted of agglomerates (Fig. 2(a)), of a characteristic size of around 10 um. Single agglomerates had a rarefied hairy structure (Fig. 2(b)) consisting of chains of solid carbon globules. Ultrasonic treatment of the material resulted in the destruction of the agglomerates into separate chains (Fig. 2(c)) consisted of carbon globules (Fig. 2(d)).

Mechanical compressing of the synthesised materials between the parallel flat contacts resulted in a disturbance of the agglomerate structure that decreased the content of voids, increased the number of globules per unit volume, and caused the emergence of new contacts between the globules and the emergence new percolation skeletons. This in turn led to an increase in the electrical conductivity of the synthesised materials (Fig. 3(c)).

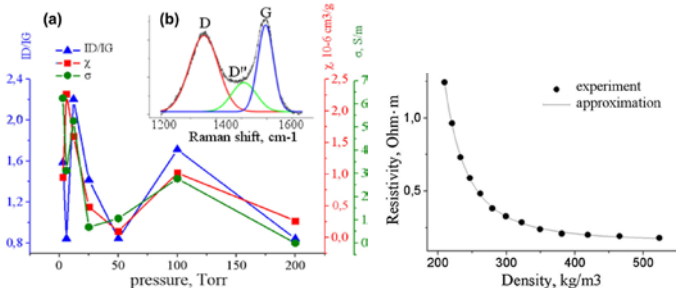

Fig.3. *(a) pressure dependence of the ID/IG ratio, the magnetic susceptibility and the electroconductivity of the synthesized materials, (b) Raman spectrum of C100, (c) density dependence of the resistivity of C12.*

According to Fig. 3(c), the resistivity of the synthesised materials decreases as the density increases. This dependence is approximated using the following power law for a system near a percolation threshold: $(\rho-\rho_0)\sim(p-p_C)^{-\gamma}$. The value ρ_0 is used to calculate the electroconductivity of the materials.

Raman spectroscopy is a robust analysis method for carbon structures. Fig. 3(b) shows the characteristic spectrum of the synthesised materials. The presence of peaks at 1350 cm^{-1} and 1584 cm^{-1} is evidence of the presence of a graphite structure. Peak G (1584 cm^{-1}) corresponds to oscillations of the bonds between the sp^2-hybridised carbon atoms, although this does not constitute firm evidence of the presence of carbon rings. However, peak D (1350 cm^{-1}) corresponds to breathing oscillations in the six-membered rings of the carbon atoms and appears on the free edges and defects of the graphene planes [26]. D" (1510 cm^{-1}) is associated with the presence of amorphous carbon [27].

Fig. 3(a) shows the pressure dependencies of electrical conductivity, magnetic susceptibility and the intensity ratio of peaks D and G (ID/IG) on the Raman spectrums. As indicated by the diagram, these parameters have complex pressure dependencies, which nevertheless correlate with each other. These correlations are due to the structure of the carbon globules that are formed during nanomaterial synthesis.

The sputtering of the graphite electrodes results in a fan-shaped jet emerging from the interelectrode gap. The jet itself contains both the product of this sputtering and buffer gas atoms [2-1, 3-2]. Fig.4 shows a simplified outline of the sections of the fan-shaped jet. The temperature of the jet's axis decreases in line with the distance from the electrodes. However, condensation of the carbon vapour leads to the formation of chains, rings and clusters of carbon atoms [1]. Further coagulation leads to the formation of nanoparticles whose stable graphite-like structure forms in sufficiently hot areas of the jet (areas 1 and 2). In instances where the particle does not reach a size sufficient for the formation of the graphite-like structure, the further coagulation of such particles in area 3 leads to the formation of the amorphous soot globule structure.

The jet is unstable, leading to turbulent mixing with the buffer gas. This buffer gas already contains carbon nanoparticles, and

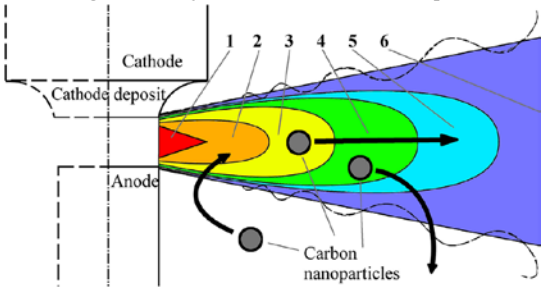

Fig.4. *Simplified outline of the jet sections: 1–jet core; 2–area of graphitisation of nanoparticles from the buffer gas; 3–area of formation of graphite-like structure; 4–area of formation of the amorphous carbon layer on the nanoparticles; 5–area of formation of globule chains; 6–area of micro-agglomerate formation.*

WEB ISSN 2535-0226
PRINT ISSN 2535-0218

should one of these enter the hot areas of the jet (area 2 on Fig. 4) the effect of the heat treatment leads either to the formation of the graphite-like structure (in the case of the graphitising structure) or an amorphous structure (Fig. 5 (a)) (in the case of the non-graphitising structure) [28]. Further movement of the nanoparticles within colder areas of the jet (area 4 on Fig. 4) may result in surface carbon deposits in the form of amorphous layers (Fig. 5(b)). Collisions of the carbon nanoparticles in even colder areas (area 5 on Fig. 4) result in the formation of chains of carbon globules (Fig. 2(c)). The formation of micro-agglomerates (Fig. 2(b)) takes place

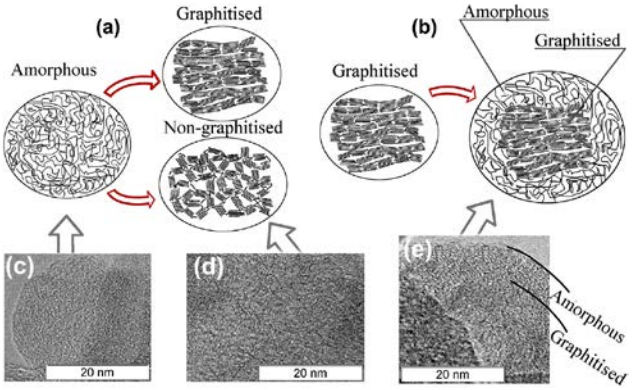

Fig. 5. *(a) transformation of amorphous nanoparticle to graphitized and non-graphitized structures (Franklin) [39]; (b) deposition of amorphous carbon layer on graphitized nanoparticle; (c) HRTEM image of amorphous carbon nanoparticle in C100; (d) HRTEM image of non-graphitized carbon structure in C100; (e) HRTEM image of amorphous carbon layer on graphitized structure in C100.*

in distant areas of the jet (area 6 on Fig. 4) and in the buffer gas.

The formation of an amorphous carbon layer on the surface of the nanoparticles with a graphite-like structure creates bonds with the atoms of the rings on the edges of the graphitic structure, reducing the intensity of peak D on the Raman spectrum. The dependence of the ID/IG ratio on the buffer gas pressure used for material synthesis also correlates with the pressure dependences of electrical conductivity and magnetic susceptibility (Fig. 3(a)).

A positive paramagnetic contribution in magnetic susceptibility is given by the structure of the free 'zig-zag' edges of the graphitic nanofragments (Fig 7(a)). The deposition of the amorphous carbon layer leads to the emergence of bonds between these 'zig-zag' edges and the amorphous layers (Fig. 7(b)), which in turn leads to a decrease in electron state density at the Fermi level. The amorphous layer on the graphitic nanofragments hence reduces the Pauli paramagnetism component for the magnetic susceptibility of the carbon nanoparticle.

The graphite-like structure has good electroconductivity due to the presence of delocalised electrons. An amorphous carbon structure with random σ- and π- bonds has a significantly weaker electrical conductivity value than a graphitic structure. The amorphous layer on the particle surface hence contributes significantly to the electrical resistivity by creating additional contact resistance between the particles with graphite-like structures.

Thus, the amorphous carbon layer on the surface of the particles with a graphite-like structure has an identical effect on the electroconductive, paramagnetic properties and ID/IG ratio of the synthesised materials, which explains the correlation of these properties (Fig. 4(a)).

In the pressure range used in the work (3–200 Torr), the jet flowing from the interelectrode gap can takes various characteristics, such as composition (C/He), speed, flow regimes, etc. The saturated vapour pressure of the carbon is 7.5 Torr at 3800K temperature, which is close to the evaporation temperature of carbon. The composition of the jet in the initial area varies from pure carbon (x(C)~100%), to the prevailing helium (x(He)>97%). The mass speeds of the anode sputtering and the cathode deposit formation were measured in the experiments. The difference in these speeds determines the speed of production of the carbon nanomaterial, which together with helium form the jet and allow determination of the speed of the jet, and the Knudsen and Reynolds numbers at the initial area of the jet. The Kn and Re exhibit values across a wide range depending on the buffer gas pressure values (Fig. 8). These jet parameters have non-monotonic dependencies on the buffer gas pressure. Thus, the pressure of the buffer gas in the reactor chamber affects the temperature and gas-kinetic parameters of the jet. Variation in the buffer gas pressure leads to the change in the size of the areas of nanoparticle formation marked in Fig. 5 and the duration of the residence of the nanoparticles in these areas.

A larger Kn for carbon atoms, which is characteristic of lower buffer gas pressures, taking into account the composition of the C-He mixture, characterises the smaller number of collisions of the carbon particles with each other and correspondingly the smaller probability of formation of carbon particles large enough for the graphite structure in the hot areas of the jet, on the one hand, and the smaller probability of precipitation of the amorphous layer on the already formed graphite-like particles in colder regions, on the other hand. A larger Re, which is characteristic of higher pressures, characterises the more intensive mixing of the jet with the buffer gas, which leads to more intensive cooling of the jet and to decreases in the size of the particle formation areas, which affects both the formation of primary particles and the deposition of the amorphous layer on the already formed graphite-like particles. In addition, the more intensive mixing of the jet with the buffer gas leads to a larger probability of the carbon particle entering from the buffer gas into the jet and therefore to heat treatment and graphitisation of the structure, when it enters into the hot areas, and to deposition of the amorphous carbon layer, when the carbon particle enters into the colder areas of the jet.

As can be seen from the complex dependencies of the electrical conductivity and magnetic susceptibility on the buffer gas pressure, gasdynamic processes have different effects on the formation of the nanomaterial structure at various pressures.

4. Conclusion

A plasma-arc synthesis of carbon nanomaterials was carried out at various buffer gas pressures. The synthesised materials are soot agglomerates at micron sizes, which consist of chains of carbon globules of nanometre sizes. Increasing the pressure of the buffer gas leads to the formation of globules of larger sizes. Nevertheless, the effect of buffer gas pressure on the internal structure is complex, which affects the electrical conductivity, the magnetic susceptibility, and the ID/IG ratio on the Raman spectrum of the synthesised materials.

At various buffer gas pressures, the helium-carbon jet flows from the interelectrode gap, with different thermal and gasdynamic characteristics, which lead to various conditions for the formation of the amorphous carbon layer on the nanoparticle surface. Nevertheless, the correlation of the dependencies of the electrical conductivity, the magnetic susceptibility and the ID/IG ratio of the synthesised materials on the buffer gas pressure indicates an affinity in the effects of the internal structure of the carbon globules on these parameters.

It was found that the values of the electrical conductivity, the magnetic susceptibility and the ID/IG ratio are affected by the amorphous carbon layer formed on the carbon nanoparticle surface with a graphite-like structure.The amorphous carbon layer forms bonds with free graphite edges, thereby reducing the value of the ID/IG ratio, including forming bonds with zig-zag edges, which reduces the paramagnetic contribution to the magnetic susceptibility, and also creates an additional contact resistance upon contact of nanoparticles, which leads to a decrease in the electrical conductivity of the synthesised carbon nanomaterials.

Acknowledgements The work was supported by grant RFBR 16-38-00322.

References

[1] .**1** O.A. Nerushev, G.I. Sukhinin, Tech. Phys**., 42**(2), pp.180-187 (1997)
[2] **2** N.I. Alekseev, G.A. Dyuzhev, Tech. Phys., **50**(11), pp.1423-1430 (2005)
[3] **3** J. H. J. Scott, S. A. Majetich, Phys. Rev. B, **52**, pp. 12564-12571 (1995)
[4] **4** D.V. Smovzh, S.Z. Sakhapov, A.V. Zaikovskii, JPCS, **754(**9), 092004 (2016)
[5] **5** A.V. Zaikovskii, V. A. Mal'tsev, S.A. Novopashin, J. Eng. Thermophys., **22(**1), pp. 77-85 (2013)
[6] **6** R.V. Gulyaev, E.M. Slavinskaya, S.A. Novopashin, D.V. Smovzh, A.V. Zaikovskii, D.Yu. Osadchii, O.A. Bulavchenko, S.V. Korenev, A.I. Boronin, Applied Catalysis B: Environmental, **147,** pp 132– 143 (2014)
[7] **7** H.Y. Yin, X.C. Song, Y.F. Zheng, X. Wang, Z.A. Yang, R. Ma, Mat Sci Eng B, **176**(8), pp. 684-687 (2011)
[8] **8** S.A. Novopashin, M.A. Serebrjakova, A.V. Zaikovskii, ARPN Journal of Engineering and Applied Science, **11**(15), pp. 9130-3133 (2016)
[9] **9** T. Makarova, F. Palacio, Carbon Based Magnetism 1st Edition An Overview of the Magnetism of Metal Free Carbon-based Compounds and Materials (Elsevier Science, Amsterdam, 2006), pp. 1- 576.
[10] **10** R.R. Gupta, In: Landolt-Börnstein New Series II/16, ed. by K.-H. Hellwege (Springer, Berlin, 1986), pp. 16-17
[11] **11** G. Wagoner, Phys. Rev., **118**, pp. 647-653 (1960)
[12] **12** J.W. McClure, Phys. Rev., **104**, pp. 666-671 (1956)
[13] **13** S. Hudgens, M. Kastner, H. Fritzsche, Phys. Rev. Lett., **33**, pp. 1552-1555 (1974)
[14] **14** S. Bandow, J. Appl. Phys., **80**, pp. 1020-1025 (1996)
[15] **15** R.C. Haddon, A. Pasquarello, Phys. Rev. B, **50**, pp. 16459-16463 (1994)
[16] **16** L. Liu, G.Y. Guo, C.S. Jayanthi, S.Y. Wu, Phys. Rev. Lett., **88**, 217206 (2002)
[17] **17** K. Wakabayashi, M. Fujita, K. Kusakabe, K. Nakada, Czechos. J. Phys., **46**, pp. 1865-1866 (1996)
[18] **18** K. Kobayashi, Phys. Rev. B, **48**, pp. 1757-1760 (1993)
[19] **19** K. Yoshizawa, K. Okahara, T. Sato, K. Tanaka, T. Yamabe, Carbon, **32**, pp. 1517-1522 (1994)
[20] **20** W. Pauli, Z. Phys, **43**, pp. 601–623 (1927)
[21] **21** H.W. Kroto, J. R. Heath, S.C. O'Brien, R. F. Curl, R. E. Smalley, Nature, **318** (6042), pp. 162–163 (1985)
[22] **22** D.V. Smovzh, I.A. Kostogrud, S.Z. Sakhapov, A.V. Zaikovskii, S.A. Novopashin, Carbon, **112**, pp. 97-102 (2017)
[23] **23** Z.S. Wu, W. Ren, L. Gao, J. Zhao, Z. Chen, B. Liu, D. Tang, B. Yu, C. Jiang, H.M. Cheng, ACS Nano, **3**(2), pp. 411-417 (2009)
[24] **24** S. Iijima, Nature, **354**, pp. 56 – 58 (1991)
[25] **25** A.E. Belikov, A.V. Zaikovsky, V.A. Maltsev et. al., Thermophys. Aeromech**., 16(**4), pp. 647-650 (2009)
[26] **26** A. C. Ferrari, J. Robertson, Phys. Rev. B, **61**, pp. 14095-14107 (2000)
[27] **27** A. Cuesta, P. Dhamelincourt, J. Laureyns, A. Martinez-Alonso, J.M.D. Tascon, Carbon, **32**, pp. 1523–1532 (1994)
[28] **28** R.E. Franklin, Proceedings of the Royal Society of London A, **209**, pp.196–218 (1951)